2261

Electro-optically controlled beam deflection and switching via total internal reflection at a domain-engineered interface in $LiNbO_3$

Alexander J Boyland*, Sakellaris Mailis, Jason M Hendricks, Peter G R Smith, Robert W Eason.

Optoelectronics Research Centre

University of Southampton

Southampton

SO17 1BJ

UK.

* corresponding author

Tel 023 80594527: Fax 023 80593142 : e-mail **ajb@orc.soton.ac.uk**

Proceedings for International workshop on periodic microstructured nonlinear optical materials - Madrid 10-13 June 2001

Abstract

We report a novel beam deflection and switching method that occurs due to the electro-optic effect under applied field when a beam at grazing incidence is incident on an interface between anti-parallel domains in a sample of $LiNbO_3$. We present data obtained for wavelengths of 0.543 μm and 1.52 μm and compare this with theoretical models. For deflection, improvements can be obtained for both range of angular deflection and transmission uniformity, by faceting the exit face of the device at an optimum angle. A theoretical analysis is presented for this configuration and compared with data obtained for a wavelength of 1.52μm. A practical geometry would permit a deflection of ~140mrad for an applied voltage of 1kV. For switching there are many attractive properties, as TIR is a 100% efficient process this leads to the possibility of high contrast ratios; current data shows contrast ratios greater than 100:1 (20dB). Other properties include relatively simple fabrication procedure, low drive voltages and a wavelength dependence that is less than other electro-optic devices such as Pockels cells.

1. Introduction

A novel beam deflection and switching technique [1] has been developed that utilises the electro-optic effect to induce a change in the refractive index, Δn, at a boundary between two domain regions in a material that has been domain-engineered so that the regions are anti-parallel. When a beam is incident on this interface at grazing angle incidence, and the difference in refractive indices of the oppositely oriented domains is increased, the beam will be deflected from its original path, with the deflection increasing with the applied field. At a suitably large angle, total internal reflection can occur for a sufficiently large difference in the refractive indices.

This novel method of electro-optically induced deflection and TIR can achieve high contrast switching, and when compared to existing techniques exhibits many advantages. The use of electro-optic deflection across a boundary rather than reflection at an interface has been reported previously, and the most reported method to date has involved prism type geometries [2-3], where light is incident on a series of triangular domain-inverted regions, and the deflection achievable is dependant on the geometry and number of the prisms. As the linear electro-optic effect in $LiNbO_3$ and $LiTaO_3$ is comparatively weak, even when using field strengths of ~$1kVmm^{-1}$, the deflection angles achievable are small. However, for grazing incidence geometries TIR can be extremely sensitive, and the larger the angle of incidence used, the lower the voltage required to induce switching. When approaching 90°, the voltage required for switching is of order only a few volts.

2. **Background**

The equation relating the applied field, E, to the induced refractive index change, Δn, due to the electro-optic effect is given by the usual expression below

$$\Delta n = -\frac{1}{2} r_{33} n_e^3 E_z \qquad (1)$$

where r_{33} is the largest electro-optic coefficient accessed by extraordinary s-polarised light, n_e is the wavelength dependent value of extraordinary refractive index, and E_z is the value of electric field applied across the sample in the z-direction.

The angle of the transmitted beam after deflection can be found by applying Snell's law at the interface, which is given by the usual expression below

$$(n + \Delta n)\sin\theta_{inc} = (n - \Delta n)\sin\theta_t \qquad (2)$$

The angle required for TIR at an electro-optically addressed interface is given by the usual expression below

$$\sin\theta_{tir} \quad \frac{n - \Delta n}{n \quad , n} \qquad (3)$$

While the coefficients relating to s-polarised light lead to better switching characteristics, switching will also occur when using ordinary p-polarised light, that

accesses the r_{13} electro-optic coefficient which has a value approximately 1/3 that of r_{33}, and n_e is replaced by n_o, the value of the ordinary refractive index.

The value used for r_{33} was 30.8 x 10^{-12} mV^{-1}[4] which was the closest published value corresponding to 0.543μm and the value for n_e was 2.23 [4] evaluated from the Sellmeier equation for a wavelength of 0.543μm.

Fig 1 shows the minimum angle required for switching to occur as a function of applied voltage. The inset shows values of Δn produced and the angle (θ_{tir}) necessary for TIR for increasing values of applied voltage for a 300μm thick sample, where Δn* is double the value of Δn calculated from (1) as the change in value of refractive index on each side of the interface is of equal and opposite sign.

3. Switch experimental details

A schematic of the electro-optically controllable domain-engineered TIR geometry can be seen in fig 2. The sample was a z-cut wafer of congruent $LiNbO_3$ of thickness 300μm, supplied by Yamaju (Japan), and had dimensions 13.5 mm x 15mm in the x and y directions respectively. The two anti-parallel domains were produced by patterning the –z face using photolithography and then electric field poling the sample. The interface was examined under a polarising optical microscope and was seen to be quite smooth, but under high magnification some variation from absolute straightness was observed. This can be seen in fig 3, which shows an example of a region of such deviation from linearity. This non-uniformity was observed for all the samples but its extent was dependent on the poling parameters used, and also varied between individual samples. The samples were annealed after poling to assist the removal of any residual strain at the interface. Even after annealing for several hours at 200°C however, a small residual refractive index of order 10^{-5} existed at the interface [1]. This residual refractive index can lead to significant Fresnel reflections at grazing angle incidence which will in turn affect the choice of incidence angle used and therefore the contrast ratio achievable.

Polarised He-Ne lasers at wavelengths of 0.543μm and 1.52μm were used to obtain experimental data. In each case the beam was spatially filtered by passing the beam through two microscope objectives (x10) and a pinhole before being focussed into the $LiNbO_3$ sample. Spot sizes of the order of 25μm for 0.543 μm light, and 64μm for 1.52μm light, were achieved by using a lens of focal length 160mm to focus the beam. Electrodes of dimensions ~12mm x 2mm were fabricated on both -z and + z

faces and were positioned across the domain interface region. The input and output faces were parallel polished and insulating supports were used to mount the device.

4. Modelling of device behaviour

The deflection of the beam can be predicted by calculating values of θ_t via (2), as a function of voltage applied across the interface. θ_t has been calculated for values of θ_i ranging from 87.7° to 89.0°, and a comparison of this data with experimental results can be seen in fig 4. It can be seen that even for modest voltages of order a few hundred volts, deflections of ~1° can be obtained. For the θ_i =87.7° the relationship is effectively linear for the voltage range 0-1000V. For the case of θ_i =88.4°, a value we have investigated experimentally and is relatively easy to implement in a sample of interface length ~10mm, a voltage of 300V (corresponding to the normalised value of 1kV mm^{-1} across the 300μm thick sample) produces an angular deflection of 0.39°. When compared to the value of angular deflection for the single prism deflector [2], we see that this near TIR geometry is ~40 times higher in sensitivity.

A 2-dimensional theoretical model was developed for predicting the switching characteristics of the TIR switch. The model can be used for any combinations of incident angle (θ_{inc}), wavelength (λ), spot size (ω_0), sample thickness (d) and wavelength dependent refractive index (n_e), as determined by the normal Sellmeier equations for $LiNbO_3$ [5].

The model can be used to characterise the beam incident on the interface for any value of angle, θ_{inc}. Fig 5 shows a schematic for the interaction of the incident beam at the interface region. For the purposes of this model the beam incident along the interface is divided into a number of slices. The lower part of the diagram shows the corresponding intensity profile; it was found that a high a level of accuracy could be

achieved by using a minimum of fifty slices. Fig 6 depicts the modelling results showing the extent to which the $1/e^2$ beam contour spreads at the interface due to the grazing angle of incidence and yields the values for where the $1/e^2$ beam profile crosses the interface. Making the assumption that the beam profile at the interface is Gaussian, the intensity profile, I, of the beam across the interface can be given for any angle of θ_{inc} using the expression

$$I = \frac{P_{total}}{l}\sqrt{\frac{2}{\pi}}\exp\left(-\frac{2z^2}{l^2}\right) \tag{4}$$

where P_{total} is the total input power of the incident beam, l is the $1/e^2$ width of the Gaussian intensity profile projected along the interface and z is the distance along the device where z=0 corresponds to the position of the beam waist. The power in each slice is given by the expression

$$P_{slice} = \frac{P_{total}}{2}\left(erf\left(\frac{\sqrt{2}x_2}{l}\right) - erf\left(\frac{\sqrt{2}x_1}{l}\right)\right) \tag{5}$$

where *erf* is the error function and x_1 and x_2 are two points that define the slice width.

There is a variation in the angle of incidence across the beam width, and this is shown in figure 7. Each slice therefore has a different effective angle of incidence, and knowing this the reflectivities of each slice can be calculated by modifying the standard Fresnel equation as applicable to fig 8 to be in terms of θ_{inc} only, which becomes

$$R_s = \left(\frac{\left[\cos\left(\sin^{-1}\left[n_{it} \sin\theta_{inc} - \cos\theta_{inc} n_{it} \right] \right) \right]}{\left[\cos\left(\sin^{-1}\left[n_{it} \sin\theta_{inc} + \cos\theta_{inc} n_{it} \right] \right) \right]} \right)^2 \quad (6)$$

where $n_{it} = n_{inc}/n_t$.

The power reflected for each slice is then calculated by multiplying the reflectivity for each slice by the power in each slice. The sum of the power of the slices that have reflectivities that fall within the parameters necessary for TIR is then calculated. This procedure is evaluated for 1000 points between 0 and 1000 Volts. The percentage of the total power is then plotted against voltage, and this allows a comparison to be made with the experimental data collected.

5. Experimental results

Fig 9 shows the geometry of interaction for the beam with the interface for all the results that follow. The $2\theta_{ext}$ angle is determined before measuring any power reflectivities and θ_{inc} is given by the expression below

$$\theta_{inc} = 90 - \theta_{int} = 90 - \left(\sin^{-1} \left(\frac{\sin \theta_{ext.}}{n_e} \right) \right) \tag{7}$$

Initially results were taken using the 0.543μm laser to characterise the presence and the strength of any residual refractive index at the interface. Powers in the reflected beam were measured at various angles with no voltage applied. The data was then superimposed onto standard Fresnel reflectivity curves and visually best-fitted to obtain values for Δn in the interface region. The values of residual refractive index difference for both polarisations on each side of the interface (given in terms of n_{it}) can be seen in table 1.

Switching data was recorded using this wavelength for both s- and p-polarised light, and these results are shown in fig 10. As expected when considering the values of the respective electro-optic coefficients accessed by each polarisation orientation, the switching of s-polarised light occurs much before that of the p-polarised light. The contrast ratio achieved was observed to be greater than 100:1 (20dB).

Switching data was also recorded at the longer He-Ne laser wavelength of 1.52μm where good switching characteristics where again observed. Detailed comparison is

now possible between the theoretical curves generated by the model, and experimental data points. As seen in fig 11 good agreement can be obtained for the early stages of switching at low applied voltages. The lack of fit as TIR is approached can be accounted for, for example, by introducing a small random angle varying between 0 and 0.2° across the interface in the numerical model to closer match the actual randomness observed for the interface. The modification to the model is then seen to generate a slight rounding off slightly close to TIR, and under suitable model parameters a closer match can be obtained to the experimental results. The contrast ratio in this case for 1.52μm light is much greater than 100:1 but the measurement of exact values is currently limited by the resolution of the apparatus used for measurement.

As previously mentioned the switch is much less wavelength dependent than other electrooptic switches such as a Pockels cell, and a comparison of voltages required for TIR for the switch and the half wave voltage, V_π , for a Pockels cell confirms this. The half wave voltage for a Pockels cell can be calculated using the expression below

$$V_\pi = \frac{\lambda}{2n_e^3 r_{33}} \tag{8}$$

where λ is the wavelength of interaction. For the TIR switch, substituting for $E_z = V/d$ where V is the voltage applied across the interface and d is the switch thickness and rearranging (1) the voltage required for TIR switching can be given by the expression

$$V = \frac{2\Delta n d}{r_{33} n_e^3} = \frac{\Delta n * d}{r_{33} n_e^3} \tag{9}$$

It is clear from (8) that the value of V_π is directly proportional to λ, in contrast to our TIR switch however, in which λ does not explicitly appear. As r_{33} and n_e and their intrinsic wavelength dispersion are common to both (8) and (9) this leads to the approximation that the TIR switch operation is effectively wavelength independent. For longer wavelength operation, there are clearly geometrical factors such as Gaussian beam focussing constraints, interface lengths required and so on, but the argument concerning effective wavelength independence is valid.

5. Further work and improvement of design

Further work includes a change to the geometry of the device when used as a beam deflector. The change enhances the performance of the device in terms of the linearity and range of the deflection angle obtained, and which simultaneously flattens the transmitted intensity characteristics. The output end of the device can be modified as in fig 12, which shows a simple modification to the output end of the sample, with the facet polished at an angle of β or γ respectively. The facet acts to magnify the angular deflection via the normal Snell law of refraction into a less dense medium, and if the angle is chosen appropriately, there is also a compensating behaviour for the previous transmission drop and the nonlinearity of angular deflection.

Figure 13(a) illustrates this behaviour for 0.543μm light at a value of $\theta_i = 87.75^\circ$ for a facet angled as shown in figure 12(a). In this geometry however, although the external angle of deflection is substantially increased when compared to that through an end face polished normally to the ray direction, the linearity is poor. Nevertheless, for $\beta = 62.5^\circ$ a deflection of ~8° is achievable for the voltage range between 0- 1000V. For the normalised value of 1kV mm^{-1} an angular deflection of 1.6° is achieved compared to a value of 0.5° without the exit facet.

When the facet is angled the opposite way, as shown in figure 12(b), then the opportunity exists to simultaneously have a large deflection range, and good linearity of deflection and transmission as a function of voltage applied. Although the linearity of deflection is not an intrinsic necessity, and can be calibrated out, it is a desirable

attribute if implementation is easy. Figure 13(b) shows calculations for this oppositely angled facet. As θ_t increases, the value of θ_γ decreases, thereby reducing the Fresnel reflectivity from this angled facet and acting to compensate for the decreasing value of transmission across the interface.

Alternative methods for device manufacture will also be investigated; these include direct bonding of two z-cut samples of $LiNbO_3$ to form a switch consisting of two oppositely oriented domains. An advantage of this technique is that it should ideally exhibit no residual strain at the domain boundary as observed for the poled domain switch, and the straightness of the interface between the two domains should also be improved dramatically by this method. Another method of switch manufacture we are keen to investigate involves the poling technique as previously described but using *stoichiometric* lithium tantalate ($LiTaO_3$) and $LiNbO_3$. This interest has arisen because manufacturers [6] report that these crystals require a lower coercive field for poling, and have higher electro-optic coefficients than the congruent materials; the coefficients for these new materials are shown in table 2. Additionally the quality of poled interfaces has been observed to be superior to those from congruent $LiNbO_3$.

6. Conclusions

In conclusion we have presented a novel electro-optic beam deflector geometry and TIR switch. The beam deflector can produce a wide angular scan range, with simultaneous capability for good linearity of both deflection angle and transmission uniformity as a function of applied field. When compared to existing schemes for electro-optic scanning based on prisms, it is seen that this new geometry has a sensitivity that is between one and two orders of magnitude larger. This geometry has been shown to function well as a beam deflector at telecoms wavelengths of ~1.5μm. The electro-optic switching technique has been shown to have good contrast ratios of greater than 100:1 (20dB), and by optimising the manufacturing method the contrast ratio could increase significantly and fulfil the potential associated with TIR (TIR is a 100% efficient process). The switch has been shown to function well at wavelengths of 0.543μm and 1.52μm. It has also been shown that the switching behaviour fits well to curves as predicted by a theoretical model.

7. Acknowledgements

The authors are grateful to the Engineering and Physical Sciences Research Council (EPSRC) for funding for AJB and JMH and for research funding via grant no. GR/N00302. Thanks also go to Kenji Kitamura, NIRIM, Japan for useful discussions and supply of stoichiometric $LiTaO_3$.

8. References

1. A J Boyland, G W Ross, S Mailis, P G R Smith, R W Eason, 'Total internal reflection switching in electro-optically addressable domain-engineered $LiNbO_3$', Electronics Letters, 37(9), p585-7 (2001).

2. J Li, H C Cheng, M J Kawas, D N Lambeth, T E Schlesinger, D D Stancil, 'Electro-optic wafer beam deflector in $LiTaO_3$', IEEE Photonics Technol. Lett., 8, p1486-1488, (1996)

3. Q.Chen, Y.Chiu, D.N.Lambeth, T.E.Schlesinger, D.D.Stancil, 'Guided-wave electro-optic beam deflector using domain reversal in $LiTaO_3$', J.Lightwave Technol, **12**, pp1401-1404, (1994)

4. R S Weis, T K Gaylord, 'Lithium niobate: Summary of Physical Properties and Crystal Structure' Applied Physics A, 37(191), p191-203(1985).

5. 'Properties of Lithium Niobate', EMIS Data Review Series No. 5, INSPEC(London), (1989)

6. Oxide Corporation datasheet. http://www.opt-oxide.com/

Table captions

Table 1 – Best-fitted residual refractive index difference on either side of the domain boundary.

Table 2 – Electro-optic coefficients and coercive fields required for domain switching for *stoichiometric* lithium tantalate and lithium niobate.

Figure captions

Fig 1 – Critical angle required for TIR as a function of voltage applied across the device of thickness 300μm. The inset shows examples of Δn produced and TIR angle implied for specific voltages.

Fig 2 – Schematic diagram for domain-engineered sample.

Fig 3 –Domain boundary as viewed using a polarising light microscope

Fig 4 – Transmitted angles θ_t as a function of voltage applied for a range of values of θ_i from 87.7° to 89.0°. Experimental results obtained for transmitted angles θ_t as a function of voltage applied for two representative values of θ_i are shown as dots.

Fig 5 – Schematic for interaction of incident beam with interface with the intensity profile of beam projected along the domain boundary for 1.52 μm light with a spot size of 64 μm incident at an angle of 89° where the intensity has been normalised such that total power under curve is equal to total power in beam

Fig 6 – Beam profile modelled at the domain boundary for 0.543 μm light with a spot size of 25 μm incident at an angle of 89°

Fig 7 – Modelled variation of incident beam angle across domain boundary for 1.52 μm light with a spot size of 64 μm incident at an angle of 89°.

Fig 8 – Schematic for Fresnel reflection at interface.

Fig 9 – Geometry of interaction.

Fig 10 – Comparison of switching for s- and p- polarisations for light of 0.543 μm incident at an angle of 88.5°

Fig 11 – Comparison of model and switching data for s-polarised light at 1.52μm incident at an angle of 89.1° (points are experimental measurements, solid line is theoretical fit)

Fig 12 – Schematic of scanners with polished exit facets. The beam exits the rear facet with angles of incidence θ_β (a) and θ_γ (b) respectively

Fig13 – (a) External angle of deflection θ_o as a function of voltage applied, for the arrangement of figure 12(a), for facet angles β between 62.5° and 64.0°. and (b) external angle of deflection θ_o as a function of voltage applied, for the arrangement of figure 8(b), for facet angles γ between 66.0° and 69.0°. The value of θ_i in both cases is 87.75°

Table 1

	'+' side	'-' side
s-polarisation	1.000046	0.999890
p-polarisation	1.000020	0.999985

Table 2

Properties	**Stoichiometric $LiNbO_3$**	**Stoichiometric $LiTaO_3$**
E-field for domain switching (coercive field) (kV/mm)	< 4	< 1.7
r_{33} electrooptic coefficients (pm/V)	38.3	35.5

Fig 1

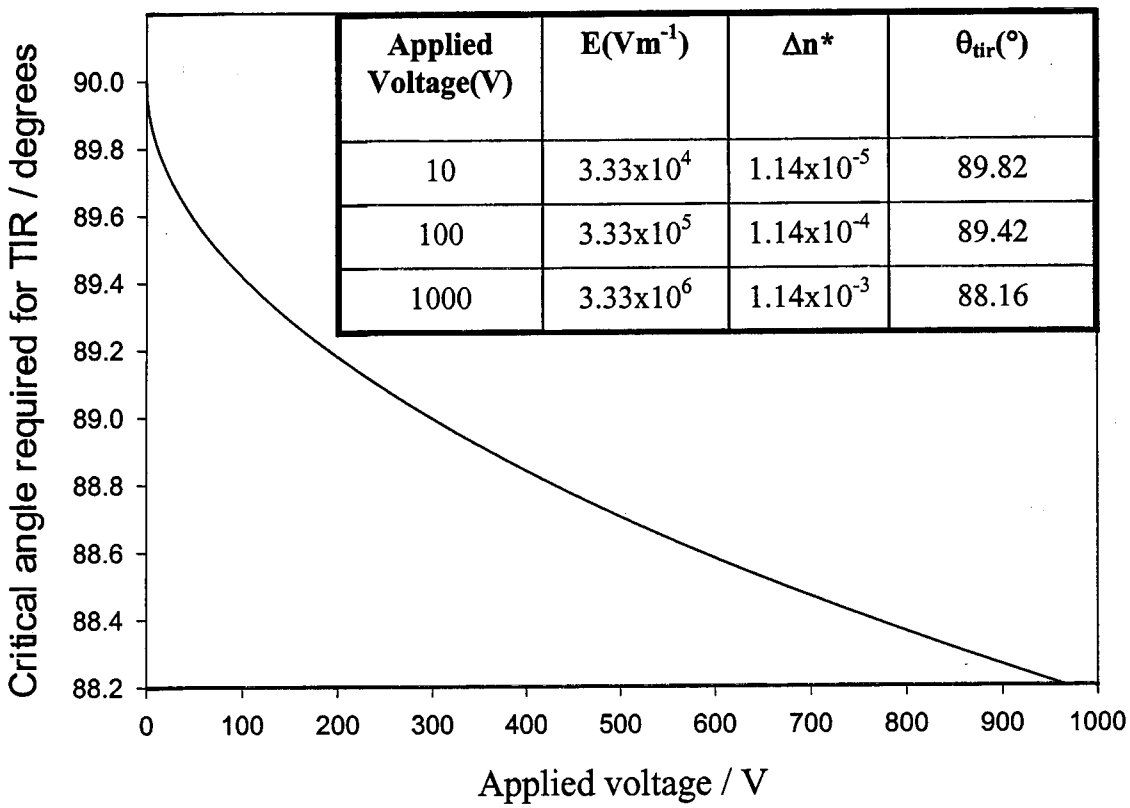

Applied Voltage(V)	E(Vm^{-1})	Δn^*	θ_{tir}(°)
10	$3.33x10^{4}$	$1.14x10^{-5}$	89.82
100	$3.33x10^{5}$	$1.14x10^{-4}$	89.42
1000	$3.33x10^{6}$	$1.14x10^{-3}$	88.16

Figure 2

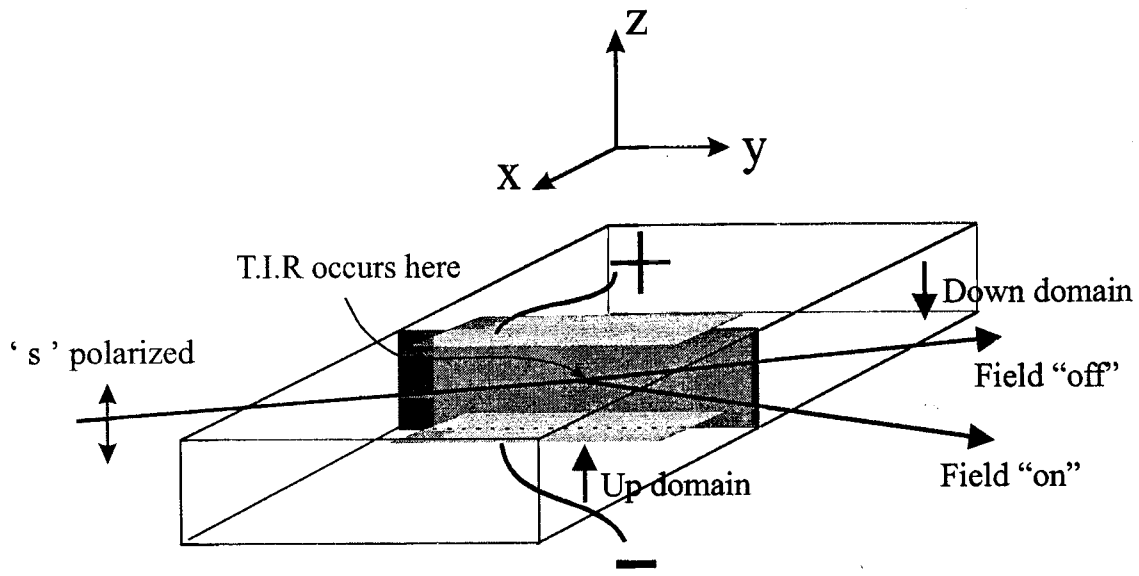
z
x
y
T.I.R occurs here
' s ' polarized
Down domain
Field "off"
Field "on"
Up domain

Figure 3

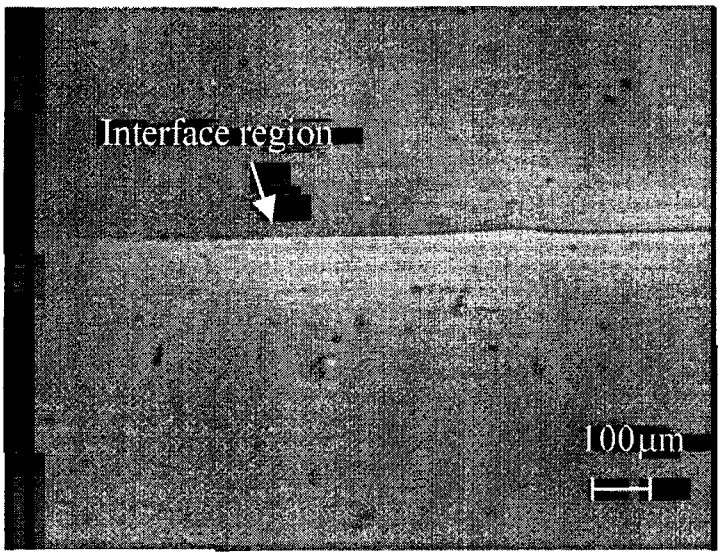

Figure 4

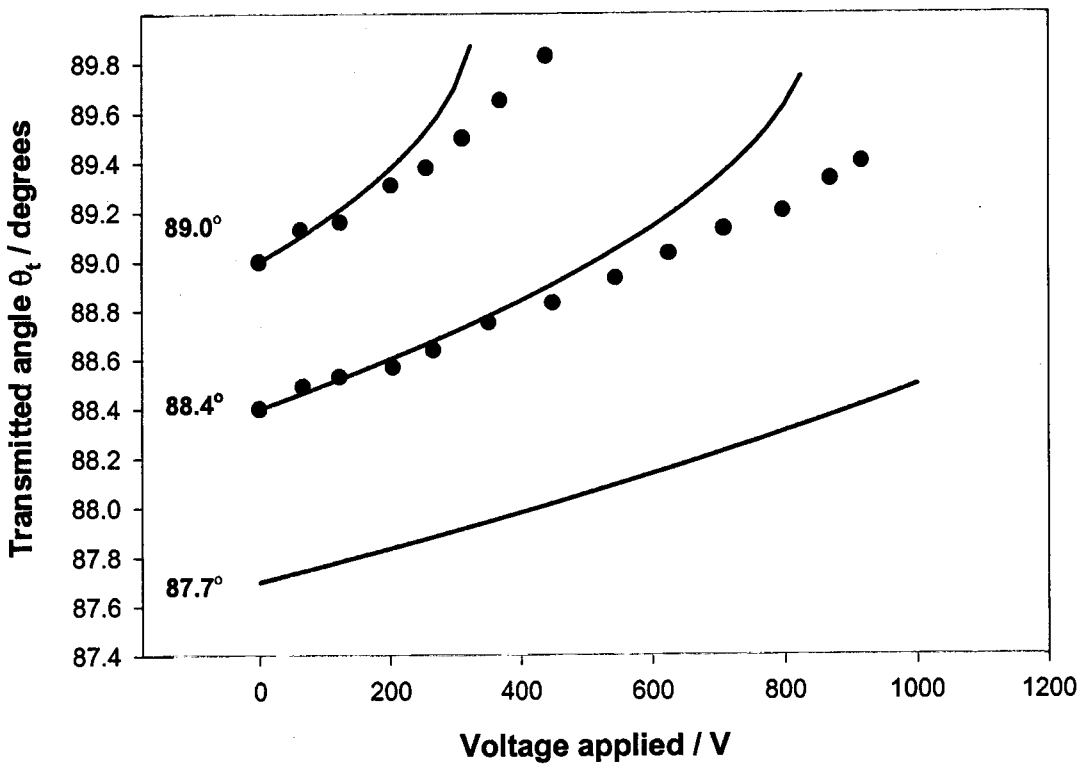
Transmitted angle θ_t / degrees
89.8
89.6
89.4
89.2
89.0
88.8
88.6
88.4
88.2
88.0
87.8
87.6
87.4
89.0°
88.4°
87.7°
0
200
400
600
800
1000
1200
Voltage applied / V

Figure 5

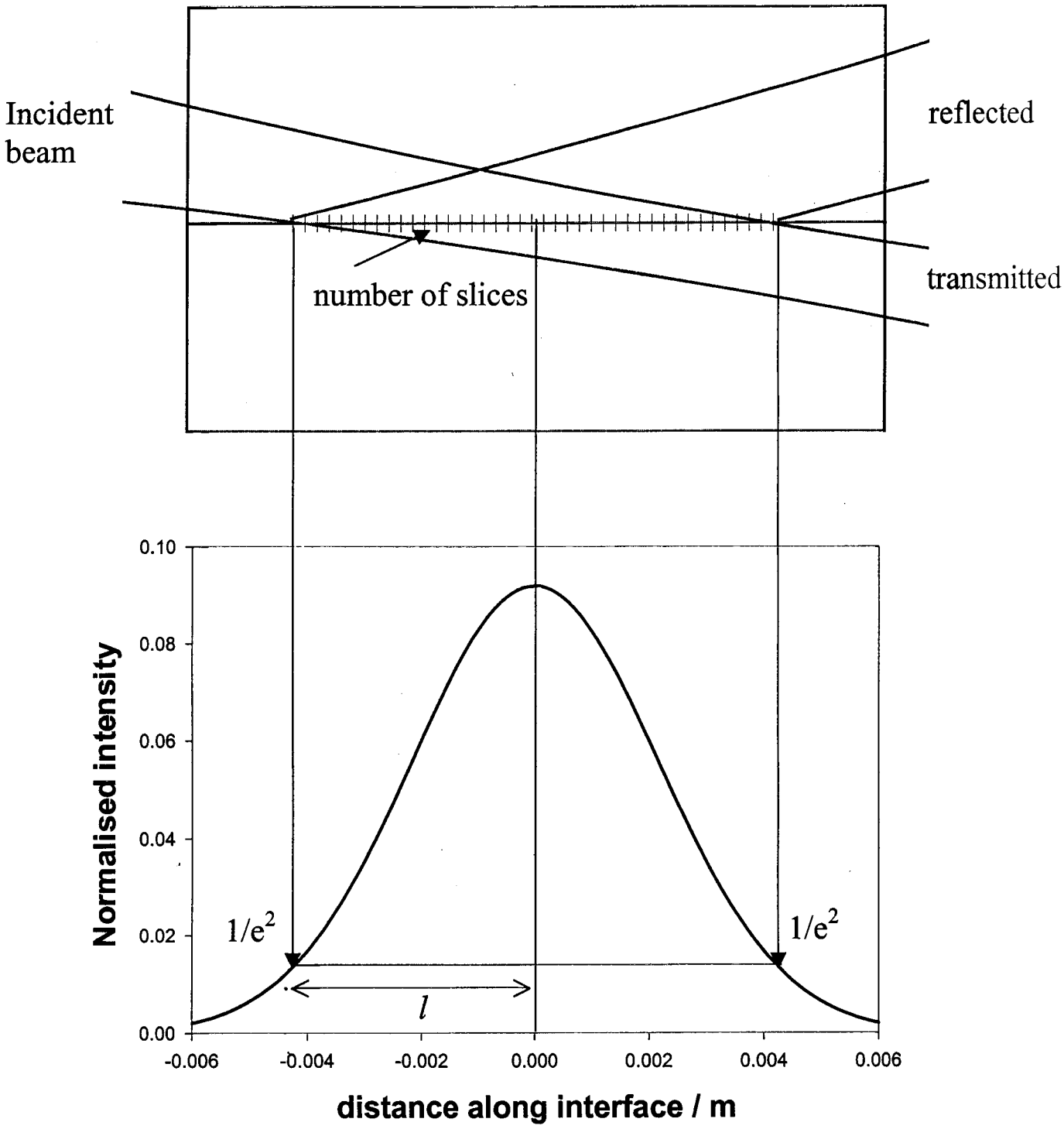
Incident beam
reflected
transmitted
number of slices
0.10
0.08
0.06
0.04
0.02
0.00
Normalised intensity
1/e2
1/e2
l
-0.006
-0.004
-0.002
0.000
0.002
0.004
0.006
distance along interface / m

Figure 6

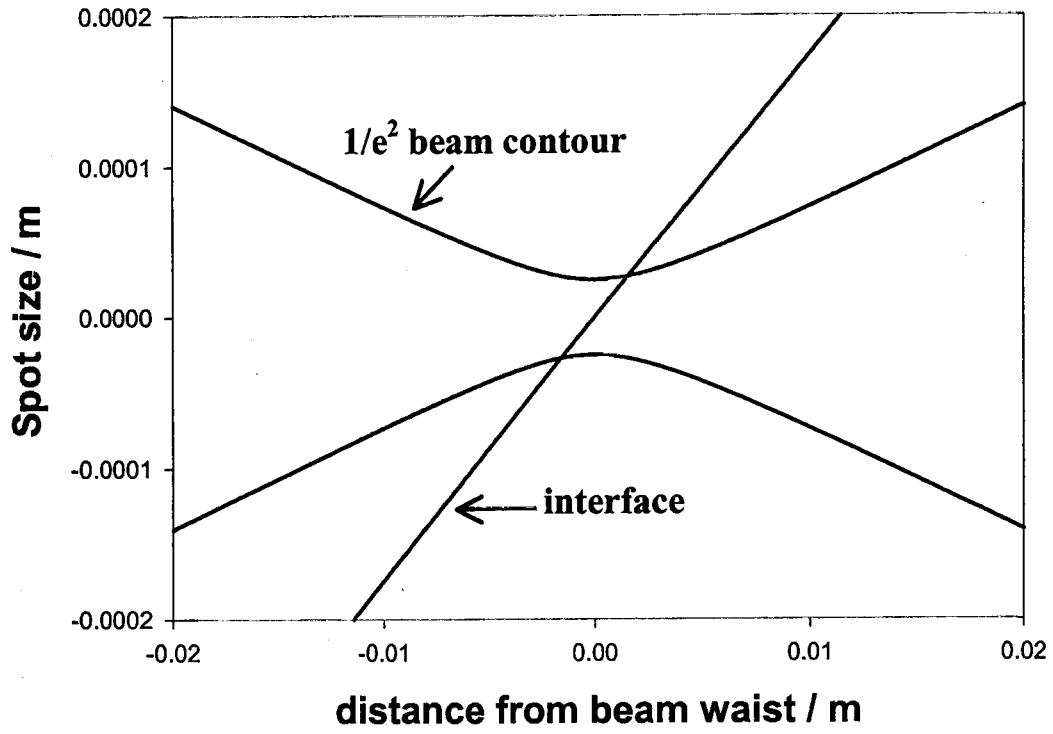
0.0002
0.0001
0.0000
-0.0001
-0.0002
Spot size / m
1/e² beam contour
interface
-0.02
-0.01
0.00
0.01
0.02
distance from beam waist / m

Figure 7

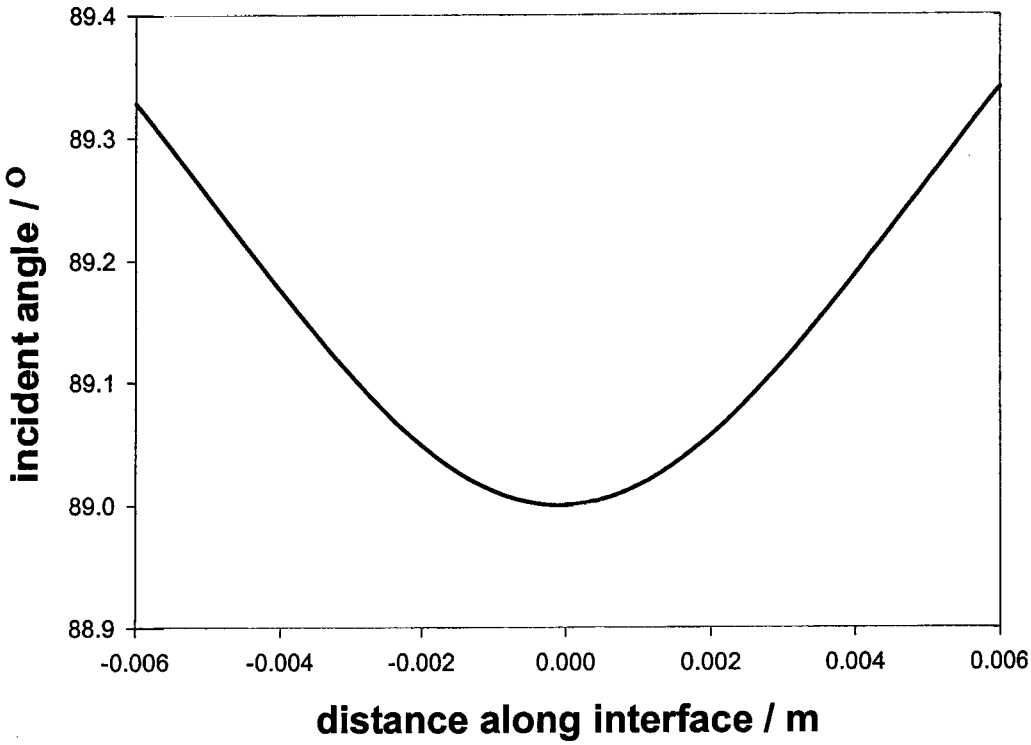
89.4
89.3
89.2
89.1
89.0
88.9
incident angle / o
-0.006
-0.004
-0.002
0.000
0.002
0.004
0.006
distance along interface / m

Figure 8

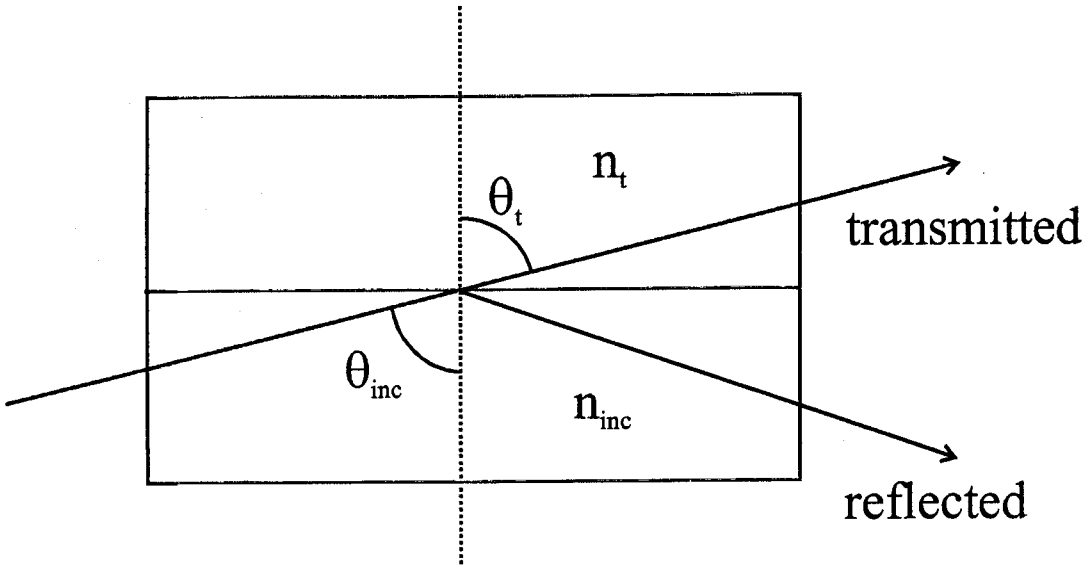

Figure 9

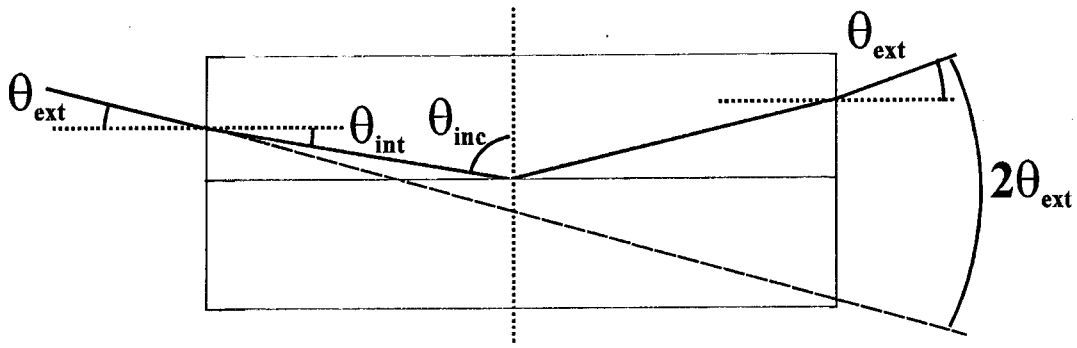

Figure 10

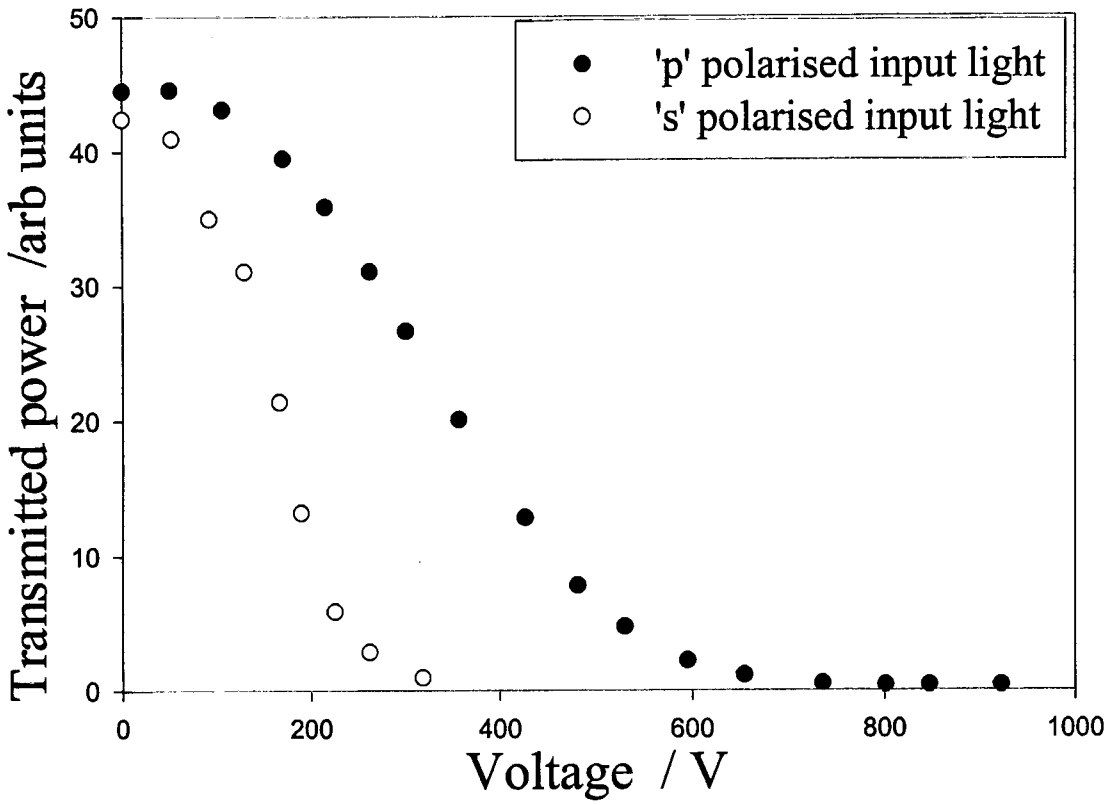
'p' polarised input light
's' polarised input light
Transmitted power /arb units
Voltage / V
0
10
20
30
40
50
0
200
400
600
800
1000

Figure 11

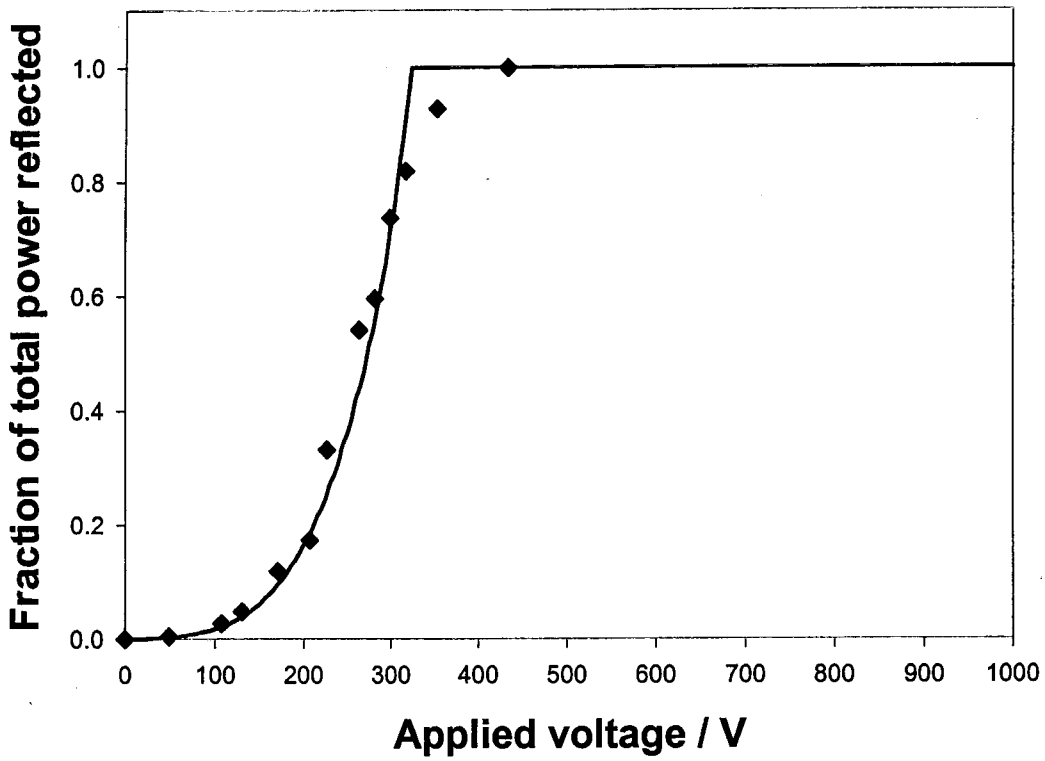
Fraction of total power reflected
1.0
0.8
0.6
0.4
0.2
0.0
0
100
200
300
400
500
600
700
800
900
1000
Applied voltage / V

Figure 12

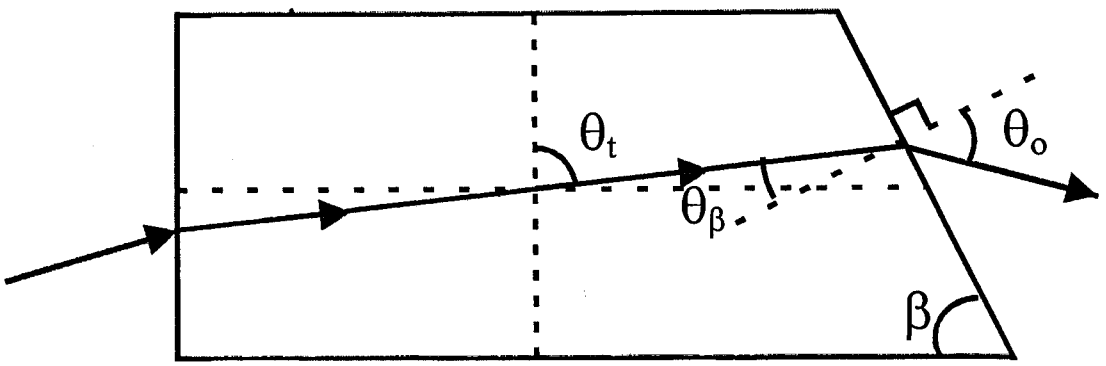

a)

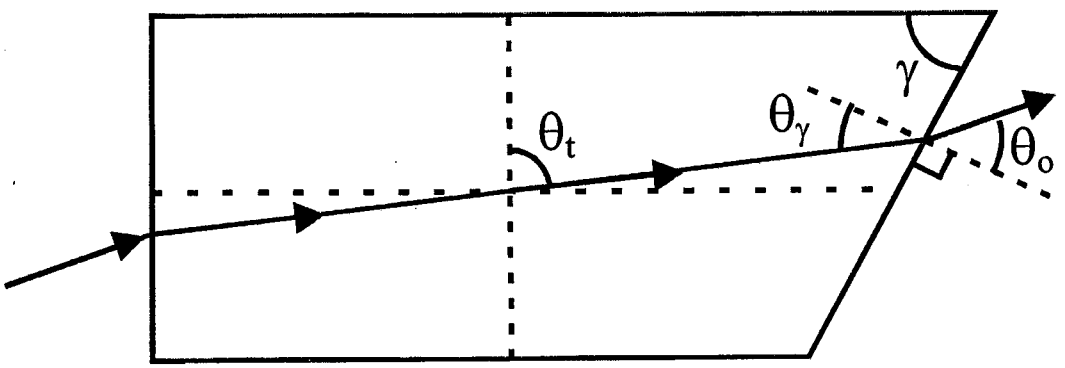

b)

Figure 13

a)

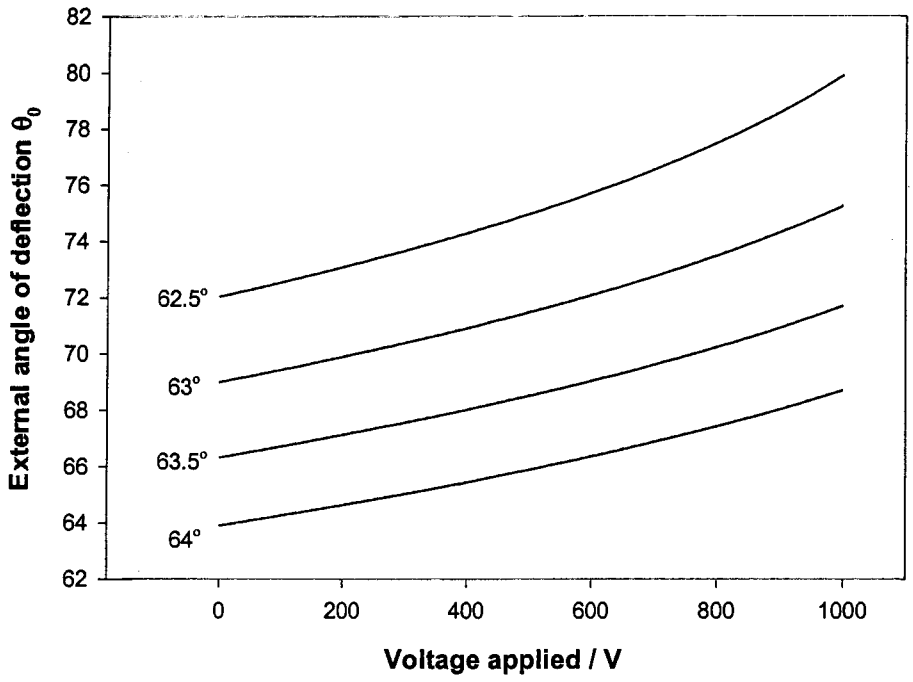
External angle of deflection θ_0
82
80
78
76
74
72
70
68
66
64
62
62.5°
63°
63.5°
64°
0
200
400
600
800
1000
Voltage applied / V

b)

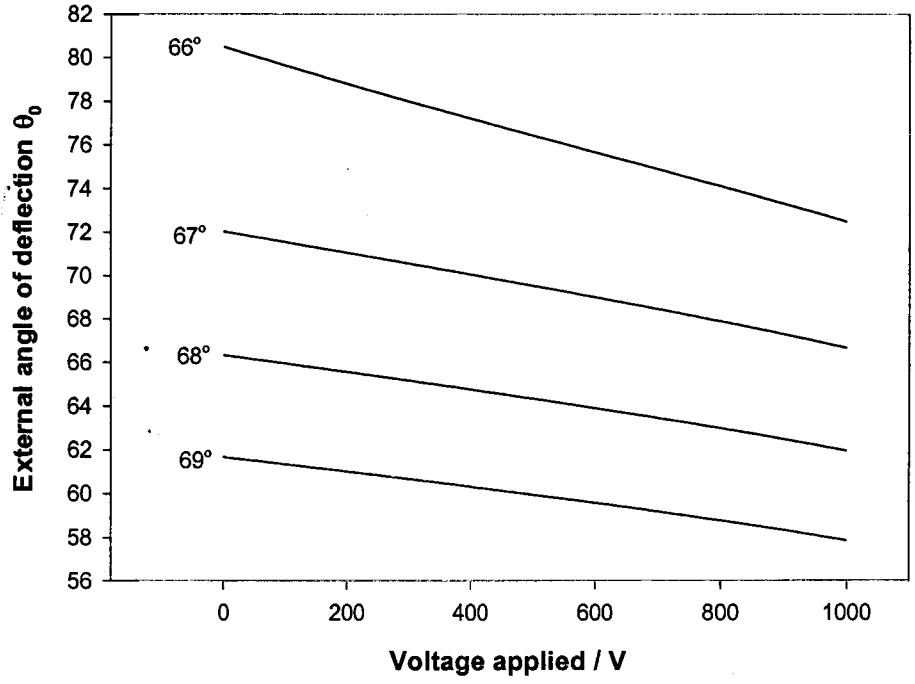
External angle of deflection θ_0
82
80
78
76
74
72
70
68
66
64
62
60
58
56
66°
67°
68°
69°
0
200
400
600
800
1000
Voltage applied / V